UNIVERSITY OF CALIFORNIA SAN DIEGO

Down Syndrome Induced Molecular and Cellular Disruption during Neurodevelopment

A Thesis submitted in partial satisfaction of the requirements
for the degree Master of Science

in

Biology

by

Hung-Hsiu Lin

Committee in charge:

Professor Hiruy Meharena, Chair
Professor Stacey Glasgow, Co-Chair
Professor Alex Chaim

2024

The Thesis of Hung-Hsiu Lin is approved, and it is acceptable in quality and form for publication on microfilm and electronically.

University of California San Diego

2024

DEDICATION

This work is dedicated to my family and friends, whose encouragement, support, and love have been the foundation of my journey.

To my incredible parents and sister, your unwavering love and support have been my guiding light. I am here today because of you.

To Dr. Meharena and Dr. Watson, thank you for seeing potential in an inexperienced undergrad. Your guidance, time, and belief in me have been instrumental in my growth as a researcher and in discovering my passion.

To Eric Zhou, your steadfast support, both emotionally and in everyday moments, has been a constant source of strength. Thank you for always being by my side.

To everyone at the DevCoGx lab, your insight, input, and assistance have been invaluable in shaping my experiments and completing my master's. Thank you for your collaboration and support.

TABLE OF CONTENTS

THESIS APPROVAL PAGE iii

DEDICATION iv

TABLE OF CONTENTS v

LIST OF FIGURES vi

ABSTRACT OF THE THESIS vii

INTRODUCTION 1

MATERIAL AND METHODS 4

RESULTS 10

DISCUSSION 19

FIGURES 22

REFERENCES 30

LIST OF FIGURES

Figure 1. Generation and Characterization of NPCs, Neurons, and Astrocytes from E21 and T21 iPSCs……..22

Figure 2. Molecular Characterization and Gene Ontology Analysis of E21 iPSC Differentiation into Neural Lineages……..23

Figure 3. Molecular Characterization and Gene Ontology Analysis of T21 iPSC Differentiation into Neural Lineages……..24

Figure 4. Characterization of Cell Cycle in E21 and T21 NPCs…… ……...……...25

Figure 5. Characterization of Size and Cell Cycle in Organoids……...…….....26

Figure 6. Characterization of Cell Differentiation Patterns in E21 and T21 NPCs Using NPC-Derived Organoids…….28

ABSTRACT OF THE THESIS

Down Syndrome Induced Molecular and Cellular Disruption during Neurodevelopment

by

Hung-Hsiu Lin

Master of Science in Biology

University of California San Diego, 2024

Professor Hiruy Meharena, Chair
Professor Stacey Glasgow, Co-Chair

Down syndrome (DS), caused by the triplication of chromosome 21, results in various physical, intellectual, and neurodevelopmental abnormalities. Despite extensive research, the precise molecular mechanisms and pathways disrupted by trisomy 21 during brain development remain largely unknown due to the complexity of the disorder and the limitations of traditional research models. However, numerous studies point to specific defects in DS neural progenitor cells (NPCs), resulting in aberrant brain development. This study examines the molecular and cellular consequences of trisomy 21 (T21) using induced pluripotent stem cells (iPSCs) differentiated into neural progenitor cells (NPCs), neurons, astrocytes, and 3D brain organoids to model early neurodevelopmental processes and cell fate decisions. RNA sequencing and gene ontology (GO) analysis revealed a disruption in neuro- and glio-genesis as well as cell cycles in NPCs. By utilizing 3D brain organoids, I also identified altered cell cycle and cell fate specification as a consequence of T21. My findings highlight the vulnerability of NPCs to T21 and suggest that differentiation is disrupted by T21.

INTRODUCTION

Aneuploidy, characterized by an abnormal number of chromosomes in a cell, is a major driver of intellectual disability disorders, among which Down syndrome (DS) is the most prevalent [1]. DS leads to a wide spectrum of physical and cognitive disabilities due to abnormal development [2]. Given its significant impact on a large proportion of newborns (1 in 750) across diverse populations, identifying the molecular and cellular mechanisms governing DS is critical for the identification of therapeutic avenues [3] for alleviating brain development abnormalities.

Neurodevelopment is an exquisitely regulated process involving neural differentiation, proliferation, and migration, resulting in the formation and maturation of key brain regions required for proper cognitive processing [4,5]. These regions, including the hippocampus, cortex, and cerebellum, are essential for learning, memory, executive functions, and motor skills [6,7]. Typical brain development involves a precise balance of cell proliferation, differentiation, migration, apoptosis, and synapse formation, establishing functional neural circuits [8,9]. In neurotypical development, neurulation, the process of neural tube formation, occurs between three-four weeks of gestation [10]. Shortly after, neural precursors proliferate rapidly and differentiate into specific neuronal cell types where deeper cortical layers are formed before the outer layers [11]. Transcription factors, such as SOX1, Tbr1, SOX9, SATB2, and GFAP are central to orchestrating these complex developmental processes, which play pivotal roles in the sequential activation required for the proper differentiation and maturation of various neuronal subtypes[12]. SOX1, for instance, marks early neural precursors, while Tbr1 and SATB2 are crucial for the specification of cortical neurons. On the other hand, SOX9 and GFAP are vital in the later stages, guiding the production of glial cells, including astrocytes, which are essential for supporting and maintaining neural function[13–

[15]. Together, these factors ensure that neurogenesis proceeds correctly, followed by the generation of glial cells, which are critical for a healthy and functional nervous system[12,16,17].

In contrast, DS is characterized by defects in neurodevelopment, including aberrant proliferation, differentiation, and survival of NPCs, leading to changes in brain morphogenesis with structural and functional abnormalities [18–21]. These individuals exhibit a reduction in overall brain volume, affecting the cerebral grey and white matter and the cerebellum[22]. This volumetric reduction is associated with intellectual disabilities, including difficulties in learning, problem-solving, memory, and communication [19]. Studies of postmortem fetal brain samples have shown that individuals with DS have reduced proliferation and altered cellular composition, characterized by a reduced number of excitatory neurons and an increased number of astrocytes across several brain regions [20]. Fewer neurons and disrupted connectivity impair the brain's ability to process and transmit information efficiently [8]. Additionally, the increased number of astrocytes, while providing support, can create an imbalance in the neural environment, disrupting the formation and maintenance of synaptic connections [23], and further contributing to the cognitive disabilities observed in DS. It is believed that these developmental abnormalities contribute to challenges in acquiring motor skills, verbal communication, and reading difficulties, as well as memory and learning impairment [24]. Understanding the molecular mechanisms underpinning T21-induced neurodevelopmental abnormalities is crucial to gain an understanding of the clinical etiologies of DS.

Despite advancements in DS research using different model systems, the molecular mechanisms driving neurodevelopmental abnormalities in DS remain largely unknown. To understand the consequences of T21 on neurodevelopment, I utilized isogenic induced pluripotent stem cells (iPSCs) derived from an individual mosaic for T21. Isogenic iPSCs were differentiated

into neural progenitor cells (NPC), neurons, and astrocytes in addition to 3D brain organoids [25–28]. I then utilized immunostaining approaches to characterize the cells during differentiation and RNA-sequencing to gain a holistic understanding of the molecular signature of control (euploid; E21) and T21 cells throughout the early stages of neural lineage differentiation. By investigating the molecular mechanisms of aberrant NPC differentiation, I aim to understand how T21 leads to NPC dysfunction. Our findings showed that T21 leads to profound disruptions in the precise regulation of neurogenesis and cell cycle genes. By utilizing 3D organoid models, I identified that T21 affects the differentiation of NPCs. These insights deepen our understanding of Down syndrome pathophysiology and strongly suggest that the neurodevelopmental deficits associated with Down syndrome are primarily rooted in differentiation challenges.

MATERIAL AND METHODS

iPSC, NPC, Neurons, Astrocytes Generation

iPSC:

The isogenic pair of induced pluripotent stem cells (iPSCs) were purchased from WiCell (https://www.wicell.org/home/stem-cells/catalog-of-stem-cell-lines/uwwc1-ds1.cmsx https://www.wicell.org/home/stem-cells/catalog-of-stem-cell-lines/uwwc1-ds2u.cmsx). iPSCs are cultured on Matrigel in mTESR+. iPSCs were cultured to 80% confluence, at which point non-differentiated colonies were carefully selected and transferred to a feeder-free system. This transfer involved gentle dissociation using Gentle Cell Dissociation Reagent (STEMCELL Technologies, cat#100-0485) to lift the colonies from the Matrigel surface, ensuring minimal disruption to cell integrity. The cells were then grown on Matrigel hESC-Qualified Matrix coated plates (VWR, 354277) using mTeSR+ medium (Stemcell Technologies, 85850). Medium changes were performed daily, and cells were passaged every three to four days, depending on the confluency and growth rate.

NPC:

iPSCs were grown to 80% confluence in mTeSR1 medium (STEMCELL Technologies, cat#85850) and then dissociated into a single-cell suspension using Gentle Cell Dissociation Reagent (STEMCELL Technologies, cat#100-0485). 3 million cells were transferred into a single well of AggreWell 800 (STEMCELL Technologies, cat#34811) to form 300 embryoid bodies (EBs) of 10,000 iPSCs each in STEMdiff Neural Induction Medium + SMADi (STEMCELL Technologies, cat#05835). Half-medium replacement was performed daily for 4 days. On day 5, EBs were transferred onto matrigel-coated plates (Sigma, cat#P6407), and complete medium replacement was performed daily for 10 days. On day 15, neural rosettes were isolated using

STEMdiff Neural Rosette Selection Reagent (STEMCELL Technologies, cat#05853) and re-plated onto fresh matrigel-coated plates in STEMdiff Neural Induction Medium + SMADi. Complete medium replacement was performed daily for 6 days. On day 21, NPCs were ready for sequencing and staining.

Neurons:

Neurons were generated by introducing the inducible NGN2 transgene into the AAVS1 safe harbor locus using TALENs. Plasmids were obtained from Addgene (iNGN2: #124229, R TALEN: #62197, L TALEN: #62916), sequences were confirmed by Sanger sequencing, and purified by maxi-prep using PureLink HiPure Plasmid Maxiprep Kit (Thermo Fisher Scientific #K210007). E21 and T21 iPSCs were transfected with all three plasmids using Lipofectamine Stem (Thermo Fisher Scientific), and positive clones were selected using blasticidin. After selection, iNGN2-E21 and iNGN2-T21 iPSCs were differentiated into NPCs using methods previously described, prior to doxycycline (DOX) treatment to induce the NGN2 transgene. Three weeks post-DOX induction, neurons were fixed for immunostaining analysis, and RNA was isolated for further study.

Astrocyte:

NPCs were maintained and passaged weekly, with cells used for differentiation at passages 3 to 5. To initiate astrocyte differentiation, NPCs were treated with Astrocyte Differentiation Basal Medium (ADBM), which was prepared by supplementing Neurobasal Medium (Gibco, cat#12348017) with N2 Supplement (Gibco, cat#17502-048), GlutaMAX (Gibco, cat#35050079), Non-Essential Amino Acids (NEAA; Gibco, cat#11140050), and Penicillin-Streptomycin (Gibco, cat#15140163). The medium was further supplemented with 10 ng/mL CNTF (R&D Systems, cat#257-NT-010) and 10 ng/mL BMP4 (R&D Systems, cat#314-BPE). The NPCs were then plated

on Matrigel-coated plates and cultured in this medium for 21 days, with media changes every 2-3 days, to promote astrocyte differentiation. After 21 days of differentiation, the cells were prepared for subsequent experiments, including further analysis of astrocyte characteristics.

Generation of organoid

NPCs were dissociated into single cells and plated at a density of approximately 100,000 cells per well in 96-well round-bottom ultra-low attachment plates (Corning) in NPC-expansion medium [1:1 mix of DMEM/F-12 + GlutaMAX (Gibco, cat#10565018) and Neurobasal (Thermo Fisher Scientific, cat#21103049), supplemented with N2 Supplement (Gibco, cat#17502-048), B27 Supplement with vitamin A (Gibco, cat#12587010), GlutaMAX (Thermo Fisher Scientific, cat#35050-079), MEM non-essential amino acid solution (Sigma-Aldrich, cat#M7145), and Pen/Strep (Gemini Bio-Products, cat#400-109)]. The medium was changed twice a week, and cells were fixed with 4% paraformaldehyde in 1X PBS on different dates (d30, d180).

Immunofluorescence Staining

Cells grown on coverslips were fixed with 4% paraformaldehyde in 1X PBS for 10 minutes, then incubated overnight at 4°C in primary antibody diluted in 1X PBS with 0.3% Triton X-100. Coverslips were washed three times with PBS and then incubated with Alexa-Fluor 488, Alexa-Fluor 555, and Alexa-Fluor 647 secondary antibodies (1:1,000 dilution) and DAPI (1:1,000 dilution) for 10 minutes at room temperature. The coverslips were mounted on microscope slides using Fluoromount, and the slides were imaged using a confocal microscope with a 20x or 60x objective, with identical settings applied for paired images.

RNA sequencing

Biological replicates (n=3) of the isogenic pair of iPSCs and their derived NPCs, neurons, and astrocytes were used for RNA-seq library preparation. RNA was extracted using the RNeasy Kit for RNA purification (Qiagen, cat#74104) following the manufacturer's instructions and was sent to sequencing. Differential gene expression analysis was performed using DESeq2. Significant differentially expressed genes (DEGs) were identified with a false discovery rate (FDR) of less than 0.001 and a log2 fold change threshold of ±0.3. Gene ontology and enrichment analyses were conducted in R using custom scripts. In these analyses, a randomized permutation test was employed, where a sample set of the same size as the observed data was randomly selected from the background set. The statistical test was then applied to each randomly sampled dataset in the same manner as the observed data, providing the enrichment results. To visualize the results of the differential gene expression analysis, heatmaps and volcano plots were generated using R. Heatmaps were created where normalized gene expression values (obtained from DESeq2) were scaled and clustered using hierarchical clustering. For volcano plots, the "ggplot2" package was used. Log2 fold changes were plotted on the x-axis, and the negative logarithm of the FDR-adjusted p-values on the y-axis, with a custom color scheme applied to highlight DEGs that passed the significance thresholds.

Click-IT EdU with Immunostaining

Cells were labeled with EdU by adding a 10 mM EdU stock solution, prepared by dissolving 5 mg of EdU in 2 mL DMSO, to the culture medium at a final concentration of 10 µM. The cells were incubated with EdU for 3 hours (NPC) and 24 hours (organoids) for pulse labeling. Following EdU incorporation, cells were fixed with 4% paraformaldehyde (PFA) in PBS for 10 minutes at room temperature, then washed three times with PBS. The Click-iT reaction was performed by first permeabilizing the cells with 0.3% Triton-X in PBS for 20 minutes at room

temperature. During permeabilization, a Click-iT Reaction Cocktail was prepared by diluting the 10X Click-iT reaction buffer to a 1X working solution. The reaction cocktail was then applied to the cells by placing the coverslips face down onto droplets of the cocktail on a parafilm surface, and the cells were incubated in the dark for 30 minutes at room temperature. After washing the cells three times with PBS containing 0.3% Triton-X, immunostaining was performed. Cells were incubated with primary antibodies diluted in PBS with 0.3% Triton-X overnight at 4°C with gentle rocking. Following three washes with PBS, secondary antibodies conjugated to unique fluorophores were applied for 1 to 2 hours at room temperature. After washing, cells were incubated with DAPI solution (1 µg/mL final concentration) for 10 minutes at room temperature to stain the nuclei. Finally, cells were washed three times with PBS, mounted with Fluoromount-G, and sealed with nail polish for imaging.

Image Analysis

All image analyses were conducted using ImageJ (FIJI). The differentiation efficiency of NPCs was determined by calculating the ratio of SOX1-positive cells to the total number of nuclei, as identified by DAPI staining. Similarly, the differentiation efficiency of iPSCs was assessed by calculating the ratio of SOX2-positive cells to the total number of DAPI-stained nuclei. The proportion of EdU-positive cells was quantified by counting the EdU-positive cells and dividing by the total number of DAPI-stained nuclei.

For the analysis of immunostaining in organoids, we employed an in-house analysis pipeline. For nuclear staining, a custom ImageJ macro was developed to create a DAPI mask, setting thresholds specific to each immunostaining channel based on the marker being analyzed. The resulting data were then imported into R for further analysis, where the percentage of cells

expressing a specific marker relative to the total number of DAPI-positive nuclei was calculated to assess marker expression.

For non-nuclear staining, such as GFAP, a FIJI macro was used to isolate the GFAP-positive area within the organoid. The GFAP-positive area was then divided by the total area of the organoid to determine the percentage of the organoid occupied by GFAP expression.

Organoid size analysis was also performed using a FIJI macro, which isolated the organoid and provided precise measurements of its size. This comprehensive image analysis approach ensured accurate quantification of differentiation efficiency, marker expression, and organoid size across all experiments.

RESULTS

Generation and Characterization of NPCs, Neurons, and Astrocytes from E21 and T21 iPSCs

To validate the generation of the desired cell types, including NPCs, neurons, and astrocytes from euploid (E21) and trisomy 21 (T21) iPSCs (Figure 1A), we utilized immunohistochemistry with cell type-specific markers (Figure 1B). For iPSCs, we stained for SOX2 and Nanog, which are key markers of pluripotency and the undifferentiated state. For NPCs, we utilized SOX1 and Nestin; SOX1 is a transcription factor marking early neural progenitors, while Nestin is an intermediate filament protein indicative of neural stem cells and progenitors. For neurons and astrocytes, we used MAP2 and GFAP, respectively. MAP2 (Microtubule-Associated Protein 2) is a neuron-specific cytoskeletal protein that marks mature neurons, while GFAP (Glial Fibrillary Acidic Protein) is an intermediate filament protein that marks astrocytes. Additionally, we stained for ALD1L1 and Vimentin in astrocytes, but these astrocyte-specific markers were stained only in the DS line (Figure 1B). The immunostaining results collectively confirmed the successful differentiation into the target cell types, validating our experimental approach and providing a solid foundation for further investigation into Down syndrome neurodevelopment. For both E21 and T21 iPSCs, SOX2 expression was nearly universal, with 99.9% of the cells testing positive for this pluripotency marker, indicating a high level of stemness retained during culture. Following differentiation, both E21 and T21 NPCs exhibited a differentiation efficiency rate exceeding 90%, confirming the robustness of the protocol in generating neural progenitor cells with consistent and reliable outcomes.

To gain deeper insights into the gene expression changes associated with T21, we employed RNA sequencing (RNA-seq) to analyze the transcriptomes of the cells across

differentiation. RNA-seq provides a comprehensive overview of gene expression profiles, enabling the identification of differentially expressed genes and pathways by comparing the transcriptomic data between T21 and control (E21) cells. To further characterize each cell type, we generated a heatmap from RNA-seq data displaying the gene expression profiles of specific markers for each cell type in E21. The heatmap included key genes such as OCT4 and Nanog for iPSCs, PAX6 and SOX1 for NPCs, MAP2 and NEUN for neurons, and GFAP and S100B for astrocytes (Figure 1C). These data provide strong evidence for the successful generation of NPCs, neurons, and astrocytes from both E21 and T21 iPSCs.

Molecular Characterization and Gene Ontology Analysis of E21 iPSC Differentiation into Neural Lineages

To understand the molecular behavior of E21 cells, we performed RNA sequencing on each cell type (Figure 2A) to identify gene expression changes during differentiation. RNA was extracted at specific time points for each cell type, ensuring coverage of key stages in differentiation, and sequenced to generate comprehensive transcriptomic profiles. The number of genes that were upregulated or downregulated during differentiation was visualized using volcano plots (Figure 2B), which highlighted significant changes in gene expression with a threshold of $|\log2 \text{ fold change}| > 0.3$ and an $FDR < 0.001$. We observed a higher number of differentially expressed genes (DEGs) when iPSCs differentiated into NPCs compared to when NPCs differentiated into their subsequent lineages, suggesting a major shift in transcriptional activity during the early stages of neural differentiation. DEGs were then subjected to gene ontology (GO) analysis to examine biological processes that change during differentiation (Figures 2C,D). GO analysis was performed using R, which allowed for the categorization of DEGs into biological

processes based on their functional annotations. This analysis revealed that the biological processes were divided into four distinct modules according to the behavior of genes in those categories during differentiation. Each module was characterized by distinct patterns of gene expression, offering insights into the temporal regulation of biological processes. Module 1 represented biological processes containing genes that consistently increased in expression across neural differentiation (i.e., from iPSCs to NPCs and then from NPCs to either neurons or astrocytes). These processes were enriched for genes involved in neural development, synaptic signaling, and neuronal differentiation. Module 2 represented biological processes containing genes that decreased in expression when cells differentiated from iPSCs to NPCs and then increased in expression from NPCs to either neurons or astrocytes, reflecting a biphasic pattern of gene regulation. Processes in this module included cellular metabolic processes such as lipid and cholesterol metabolism, secretion, cell motility, apoptosis, and cell death, as well as endoplasmic reticulum (ER) and Golgi functions. Module 3 represented biological processes containing genes that decreased in expression during the transition from iPSCs to NPCs, with a particular focus on translation, glycolytic processes, and mitochondrial function, indicating a shift away from pluripotency-associated metabolic activities. Module 4 represented biological processes containing genes that decreased in expression when NPCs differentiated into either neurons or astrocytes, predominantly including processes like cell cycle regulation and DNA damage response, which are downregulated as cells exit the cell cycle and mature into specialized neural cell types.

From Figure 2C, focusing specifically on neurons, we observed that genes involved in the regulation and generation of neurons increased in expression throughout differentiation (Module 1). This upregulation underscores the progressive commitment of cells to a neuronal fate and the

activation of gene networks critical for neuronal identity. Processes in Module 2 included cellular metabolic processes such as lipid and cholesterol metabolism, secretion, cell motility, apoptosis and cell death, as well as ER and Golgi functions, reflecting the cellular remodeling required for neuronal differentiation. Module 3 contained processes such as translation, glycolytic processes, and mitochondrial function, indicating a reduction in pluripotency-related metabolic activities as cells commit to a neural lineage. Module 4 included processes like cell cycle regulation and DNA damage response, highlighting the downregulation of proliferative signals as neurons mature. In Figure 2D, which characterizes astrocytes, we observe a similar pattern across all modules. Genes associated with gliogenesis consistently show an upward trend that is similar to how neurogenesis behaves during neuron differentiation, emphasizing the shared developmental cues that govern both neuronal and glial differentiation.

Molecular Characterization and Gene Ontology Analysis of T21 iPSC Differentiation into Neural Lineages

To understand the consequences of how T21 affects each module in either neurons or astrocytes, we analyzed the RNA-seq results (Figure 2A) and identified the differentially expressed genes (DEGs) by comparing E21 cells to T21 cells for each cell type (iPSCs, NPCs, neurons, and astrocytes). The DEGs were determined using DESeq2, applying a threshold of log2 fold change > 0.3 and an FDR < 0.001 to ensure robust identification of significant transcriptional changes**.** The number of DEGs was visualized using volcano plots and bar charts (Figure 3A and B), which illustrated the magnitude and direction of gene expression changes between E21 and T21 cells. These visualizations revealed a distinct transcriptional landscape influenced by T21 across

different cell types. We observed that NPCs had the largest number of DEGs, suggesting that they might be the most vulnerable cell type transcriptionally to T21 among the cell types profiled.

T21-dependent DEGs were then subjected to enrichment analysis to identify how T21 affected the genes in each module (Figure 3C). We observed a significant enrichment of T21 DEGs in module 1 (Differentiation Module) and module 4 (Cell Cycle Module). In Module 1, genes associated with neural differentiation were upregulated in T21 NPCs and subsequently downregulated in T21 neurons, suggesting an initial activation followed by an impairment in neuronal maturation. In Module 4, cell cycle regulation genes were downregulated in T21 NPCs and upregulated in T21 neurons, reflecting a disruption in the normal cell cycle exit required for differentiation. Given that cell cycle is associated with differentiation, our transcriptional analysis collectively suggests that T21 primarily manifests as a differentiation impairment, particularly affecting the transition from NPCs to mature neurons and astrocytes.

Characterization of Cell Cycle in E21 and T21 NPCs

In addition to the GO analysis, we characterized the cell cycle in E21 and T21 NPCs. Cell cycle analysis was performed using EdU incorporation assays, which measure DNA synthesis as an indicator of cells in the S phase, combined with DAPI staining to assess total cell number. We observed a decrease in the proportion of EdU-positive cells relative to DAPI area in T21 NPCs over a three-hour period (Figure 4A, B), indicating reduced proliferation. This reduction in proliferative capacity aligned with the downregulation of cell cycle-related genes observed in T21 NPCs (Figure 3C), further supporting the notion of impaired cell cycle progression in these cells. In conclusion, our findings demonstrated that T21 NPCs exhibit altered proliferation patterns, with a reduced proportion of cells in the S phase compared to E21 NPCs. This suggested that T21 may

impair NPC proliferation, potentially contributing to the broader neurodevelopmental abnormalities observed in Down syndrome.

Characterization of Size and Cell Cycle in Organoids

After examining the dynamics of the cell cycle in NPCs, I was interested in understanding how Trisomy 21 (T21) affects both the cell cycle and brain size. A brain organoid is a three-dimensional, simplified model of the brain that replicates essential structural and functional characteristics of the organ in vitro. By visualizing and quantifying the sizes of these organoids, we aimed to uncover the impact of T21 on these processes. By understanding organoid size changes over time, we can gain insights into how T21 may alter brain development.

Organoids were imaged using the EVOS system, and their sizes were quantified using Fiji software. We collected and measured organoids at three time points: 30 days (d30), 90 days (d90), and 180 days (d180), to assess overall size changes (Figure 5A). After capturing images (Figure 5B) and quantifying the sizes (Figure 5C) using image analysis software, we observed a distinct dynamic in the size changes of T21 organoids. In wild-type organoids, there was a steady growth from d30 to d180. However, in trisomy organoids, the size increased from d30 to d90 but surprisingly decreased from d90 to d180.

I hypothesized that this pattern is due to an initial proliferative phase in the organoids, followed by an apoptotic phase, both of which likely disrupt normal brain development and affect cell fate specification. To test this hypothesis, I first examined the proliferative phase by utilizing EdU staining, as described previously, over a 24-hour period in d30 T21 organoids (Figure 5D, E). I observed a significantly higher proliferation rate in d30 T21 organoids, indicated by a greater percentage of EdU-positive cells, confirming the initial proliferative phase (Figure 5E). When

assessing the specific cell types that were actively proliferating during this time, all four cell types, including neural progenitor cells (SOX1+/SOX9+), neural precursors (SOX1+/SOX9-), glial precursors (SOX1-/SOX9+), and non-precursor cells (SOX1-/SOX9-), showed a higher percentage of EdU-positive cells, indicating that the proliferative phase affects multiple cell populations.

In conclusion, the dynamic size changes in T21 organoids suggest a complex interplay between proliferation and apoptosis, which may contribute to abnormal brain development in T21. The similarity in organoid size between T21 and wild-type organoids at d30 and d180 further indicates that these phases may compensate for each other to some extent. Future studies will focus on assessing the apoptotic phase to better understand its contribution to the observed size changes.

Characterization of Cell Differentiation Patterns in E21 and T21 NPCs Using NPC-Derived Brain Organoids

To characterize neural lineage differentiation in E21 and T21 NPCs, we utilized NPC-derived brain organoids as a 3D in vitro model system, which recapitulates key aspects of human brain development. Organoids were assessed for cell type-specific marker expression through immunostaining at two critical developmental stages: day 30 (d30), which models early neurodevelopmental events such as NPC proliferation and initial neuronal differentiation, and day 180 (d180), representing more advanced stages of neurodevelopment, including neuronal maturation and glial differentiation (Figure 5A). Specifically, SOX1 was employed as a marker to identify neural progenitor cells (NPCs), while SOX9 was used to mark NPCs fated for glial lineages. To examine neuronal differentiation, we used TBR1 as a marker for early-born neurons, which are crucial for the formation of the deep cortical layers, and SATB2 as a marker for later-

born neurons that populate the upper cortical layers. Astrocyte differentiation was evaluated using GFAP, a well-established marker of astrocytes.

Our analysis revealed that there was no significant difference in the proportion of SOX1-positive cells between T21 and E21 organoids at d30, suggesting that the initial pool of NPCs was maintained in T21 organoids during early neurodevelopment. However, by d180, a notable reduction in SOX1-positive cells was observed in T21 organoids compared to controls, indicating a depletion of the NPC population as development progressed (Figure 6A, B). This decrease in NPCs at later stages may reflect premature differentiation or an altered cell cycle dynamic in T21 organoids, which could lead to an early exhaustion of the progenitor pool.

Interestingly, we observed an increase in the SOX9-positive population in d30 T21 organoids, suggesting a bias toward glial lineage commitment at an earlier developmental stage (Figure 6C, D). This early shift could indicate that T21 NPCs are more prone to differentiate into glial cells, potentially at the expense of neuronal lineage commitment.

Further analysis of neuronal differentiation markers revealed a significant increase in TBR1-positive cells in d30 T21 organoids, indicating an enhancement in the generation of early-born neurons (Figure 6E, F). By d180, there was also a marked increase in the SATB2-positive population in T21 organoids, suggesting an overall acceleration in neuronal differentiation across developmental stages (Figure 6G, H). This increase in both early and late neuronal markers could imply that T21 organoids undergo an expedited and potentially dysregulated neuronal differentiation process.

Additionally, a significant increase in the GFAP-positive population was observed in d180 T21 organoids, pointing to an elevated level of astrocyte differentiation at later stages of development (Figure 6I, J). The simultaneous increase in both neuronal and glial populations,

coupled with the depletion of NPCs, suggests that T21 organoids may experience a disruption in the tightly regulated balance between progenitor maintenance and differentiation, which is crucial for normal brain development.

Overall, these findings suggest that T21 organoids exhibit a disrupted neurodevelopmental trajectory, characterized by an accelerated and dysregulated differentiation process. This is manifested by an early depletion of the NPC pool, increased neuronal and glial differentiation, and potentially altered cell fate specification. These disruptions could contribute to the neurodevelopmental abnormalities observed in individuals with T21, such as altered cortical layer formation and increased gliogenesis, which are implicated in the pathophysiology of Down syndrome.

DISCUSSION

This study demonstrated significant neurodevelopmental disruption in T21 NPCs, neurons, and astrocytes compared to E21, revealing insights into the molecular and cellular consequences of T21 during neurodevelopment. The generation and characterization of these cell types from iPSCs, combined with RNA-seq and GO analysis across four different modules and cellular phenotype assessments, provided a comprehensive understanding of DS. We observed that NPCs exhibited the highest number of DEGs compared to other cell types, suggesting that NPCs were particularly vulnerable to the effects of T21. This vulnerability aligned with existing literature, which indicated that NPCs in DS were especially susceptible to disruptions in proliferation, differentiation, and survival, contributing significantly to the neurodevelopmental abnormalities observed in DS.

Our findings indicated that T21 primarily manifested as a differentiation impairment, particularly affecting neurogenesis, gliogenesis, and cell cycle regulation. The enrichment of DEGs in the differentiation and cell cycle modules suggested that T21 disrupted the normal balance of these processes, leading to premature or altered differentiation patterns. This was evidenced by the increased neuronal and astrocytic differentiation observed in T21 organoids, accompanied by a depletion of the NPC pool by late developmental time points. However, the question remained whether neuronal maturation was also disrupted at the cellular level. Our data suggested that while early neuronal differentiation was enhanced, the maturation process might have been altered, potentially leading to aberrant neuronal function. Further studies focusing on the expression of maturation markers, synaptic connectivity, and electrophysiological properties in T21 neurons could help elucidate the extent of these disruptions.

Additionally, another critical aspect to explore was whether modulation of the cell cycle in NPCs could rescue the observed differentiation disruptions. Given the increased proliferation rates and subsequent depletion of the NPC pool in T21 organoids, targeting specific cell cycle regulators might restore a more balanced differentiation trajectory. Experimental approaches involving the use of small molecules or drugs to modulate key cell cycle checkpoints in NPCs could have been instrumental in determining the feasibility of this approach as a therapeutic strategy.

Apoptosis also played a crucial role in shaping neurodevelopment, and its dysregulation could have further exacerbated the neurodevelopmental defects in DS. Future research should investigate whether the observed reduction in NPCs and altered differentiation patterns were accompanied by increased apoptotic activity. Quantifying apoptotic markers in T21 organoids across developmental stages could provide insights into the interplay between cell death and differentiation in the context of T21.

To build on these findings, it was essential to validate our in vitro observations in vivo, using DS mouse models or other relevant in vivo systems. Assessing whether the alterations in cell cycle dynamics, differentiation, and apoptosis observed in T21 organoids were also present in vivo would be critical for understanding their translational relevance. Such studies would help determine whether these in vitro findings accurately reflected the neurodevelopmental processes occurring in DS, thereby guiding the development of potential therapeutic strategies that could be applied in clinical settings.

In summary, this study shed light on the neurodevelopmental abnormalities in Down syndrome, emphasizing the significant vulnerability of neural progenitor cells (NPCs) and the disruptions in their differentiation processes. By identifying key areas of dysfunction, such as disrupted neuronal maturation, cell cycle dysregulation, and potential apoptosis, and proposing

targeted future research directions, we aimed to advance the understanding of these neurodevelopmental challenges and contribute to the development of strategies aimed at improving outcomes for individuals with DS.

FIGURES

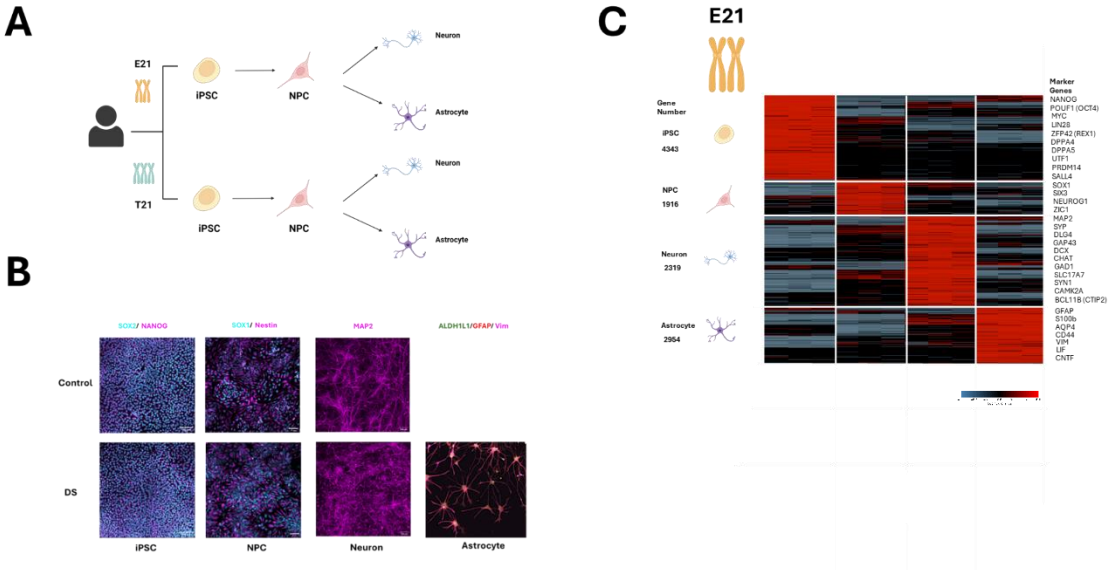

Figure 1. Generation and Characterization of NPCs, Neurons, and Astrocytes from E21 and T21 iPSCs

(A) Schematic representation of the experimental workflow outlining the differentiation of isogenic euploid (E21) and trisomy 21 (T21) induced pluripotent stem cells (iPSCs) into neural progenitor cells (NPCs), neurons, and astrocytes. The schematic illustrates the stepwise differentiation process. **(B)** Immunofluorescence staining of E21 and T21 iPSC-derived differentiated cells showing the expression of cell type-specific markers. iPSCs were stained for SOX2 (cyan) and NANOG (magenta), key markers of pluripotency, demonstrating the undifferentiated state of these cells; scale bar: 100 um. NPCs were stained for SOX1 (cyan), a marker of early neural progenitors, and Nestin (magenta), an intermediate filament protein indicative of neural stem cells and progenitors. Neurons were stained for MAP2 (magenta), a neuron-specific cytoskeletal protein that marks mature neurons. Astrocytes were stained for ALDH1L1 (green), GFAP (red), and Vimentin (magenta), highlighting the astrocytic identity of these cells. Images are presented with E21-derived cells at the top and T21-derived cells at the bottom, providing a direct comparison between the two genetic conditions. **(C)** Heatmap of gene expression profiles from RNA-seq data for cell type-specific markers in E21-derived cells with marker genes and gene numbers.

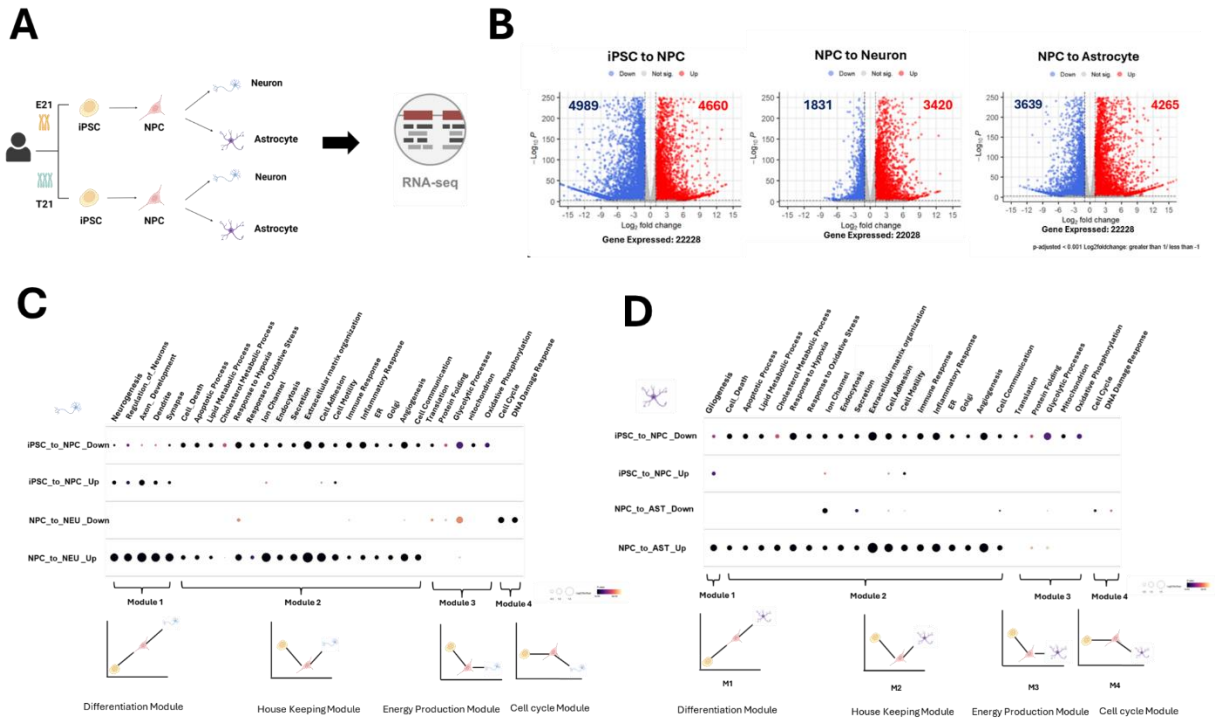

Figure 2. Molecular Characterization and Gene Ontology Analysis of E21 iPSC Differentiation into Neural Lineages

(A) Schematic of the experimental design for analyzing different cell types in isogenic E21 and T21 iPSCs, NPCs, neurons, and astrocytes. **(B)** Volcano plots visualizing gene expression changes during differentiation stages: (1) from iPSCs to NPCs, (2) from NPCs to neurons, and (3) from NPCs to astrocytes. Each plot displays differentially expressed genes (DEGs) identified by RNA-seq, with significant upregulated genes highlighted in red and downregulated genes in blue. **(C)** Module of differentially expressed genes during differentiation from iPSCs to NPCs and from NPCs to neurons, with GO categories divided into modules 1, 2, 3, and 4. **(D)** Module of differentially expressed genes during differentiation from iPSCs to NPCs and from NPCs to Astrocytes, with GO categories divided into modules 1, 2, 3, and 4.

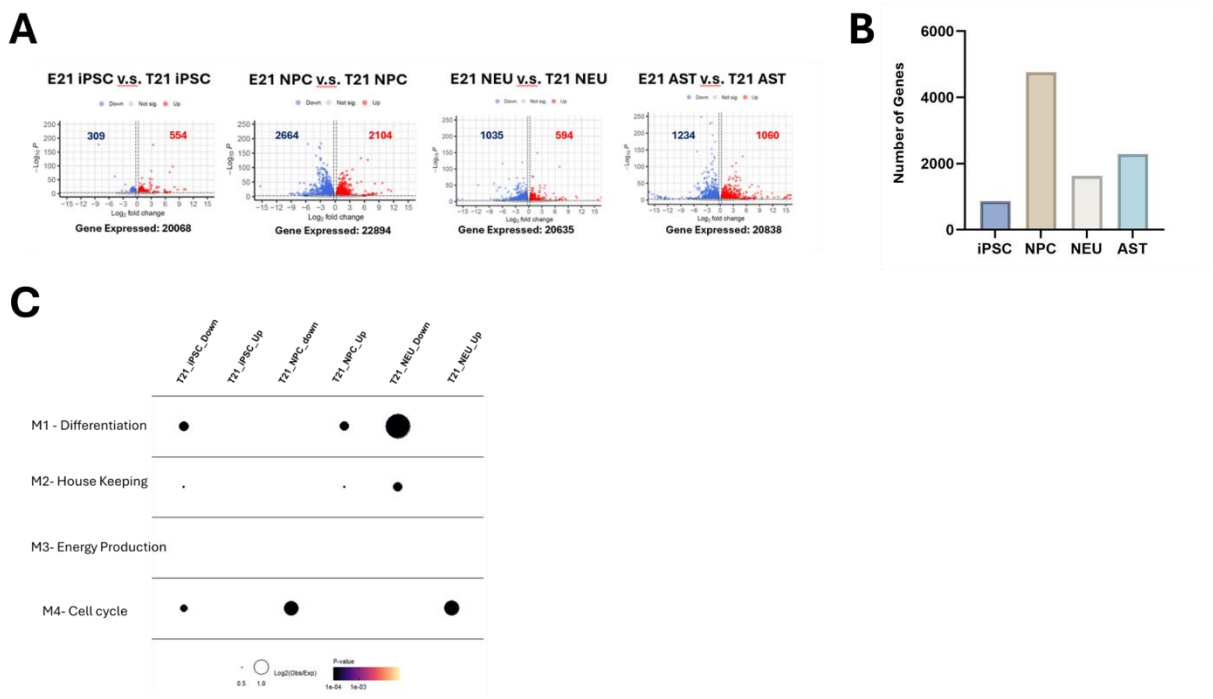

Figure 3. Molecular Characterization and Gene Ontology Analysis of T21 iPSC Differentiation into Neural Lineages

(A) Volcano plots displaying the differentially expressed genes (DEGs) identified by RNA-seq in four different cell types: (1) iPSCs, (2) NPCs, (3) Neurons, and (4) Astrocytes. Each plot highlights the significant DEGs between T21 and E21 cells, with upregulated genes shown in red and downregulated genes in blue. **(B)** Bar charts quantifying the total number of DEGs for each cell type, illustrating the relative magnitude of transcriptional changes induced by T21.**(C)** Bubble plot illustrating the enrichment of T21-dependent DEGs across various biological processes, categorized by module-specific associations. The size of each bubble represents the number of DEGs within a given module, while the color indicates the level of enrichment significance.

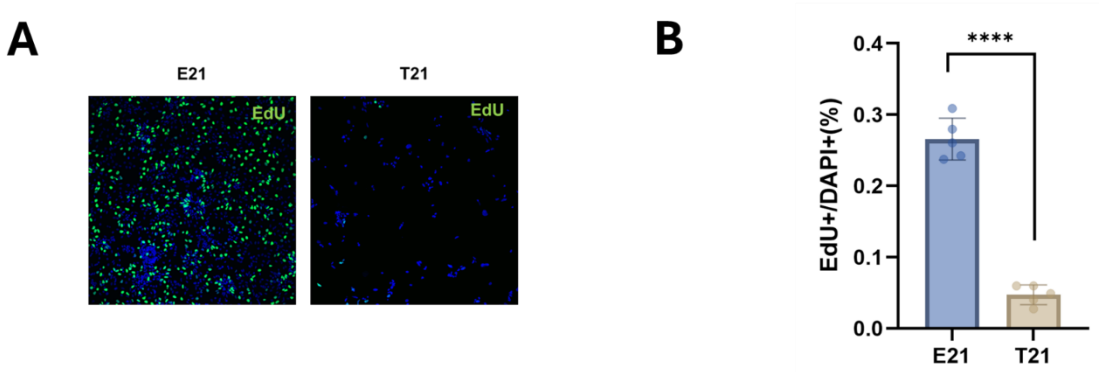

Figure 4. Characterization of Cell Cycle in E21 and T21 NPCs
(A) Immunofluorescence staining of EdU-incorporated cells (green) and DAPI-stained nuclei (blue) in E21 (left) and T21 (right) NPCs, showing the distribution of proliferating cells within the population. **(B)** Quantification of EdU-positive cells relative to the total number of DAPI-stained nuclei in E21 (left) and T21 (right) NPCs, indicating the percentage of cells undergoing DNA synthesis. Data are presented as mean ± SD, with n = 5 images per condition.

Figure 5. Characterization of Size and Cell Cycle in Organoids
(A) Schematic illustration of the experimental timeline, outlining the generation and fixation dates for E21 and T21 organoids at three developmental stages: day 30 (d30), day 90 (d90), and day 180 (d180). **(B)** Representative images of E21 and T21 organoids at d30, d90, and d180 captured using the EVOS imaging system, highlighting morphological differences over time. **(C)** Quantification of organoid size for E21 and T21 organoids at d30, d90, and d180 obtained from EVOS images. The data illustrate the growth dynamics and size variation between the two genotypes across the three time points. **(D)** Immunofluorescence staining for EdU-incorporated cells (green) and DAPI-stained nuclei (blue) in E21 (top) and T21 (bottom) organoids at d30, following a 24-hour EdU pulse. The images show the distribution and intensity of EdU incorporation, indicating proliferative activity within the organoids. **(E)** Quantification of EdU-positive cells relative to total DAPI-stained nuclei in E21 (top) and T21 (bottom) organoids at d30, reflecting differences in cell proliferation between the two genotypes. Data are expressed as mean ± SD, with n = 5 images per condition. **(F)** Quantification of EdU-positive cells stratified by specific cell types within the organoids, highlighting differences in proliferative rates among various cell populations. Data represent the mean ± SD, with n = 5 images per cell type.

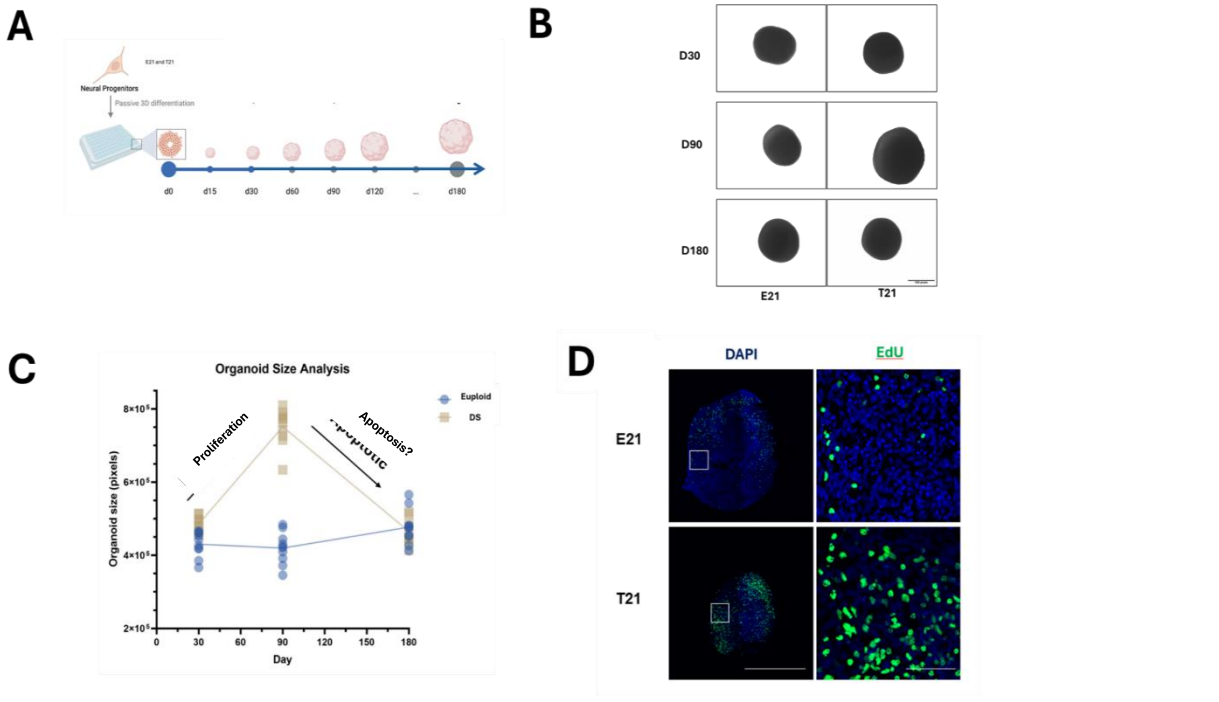
A
Neural Progenitors
Passive 3D differentiation
d0
d15
d30
d60
d90
d120
d180
B
D30
D90
D180
E21
T21
C
Organoid Size Analysis
Euploid
DS
Proliferation
Apoptosis?
Organoid size (pixels)
Day
D
DAPI
EdU
E21
T21
E
EdU+/DAPI+(%)
E21
T21
F
Percent (EdU%)
Neural Pregenitor Cells (SOX1+/SOX9+)
Neural Precursor Cells (SOX1+/SOX9-)
Glial Precursor Cells (SOX1-/SOX9+)
Non-Precursor Cells (SOX1-/SOX9-)
ns
ns

Figure 6. Characterization of Cell Differentiation Patterns in E21 and T21 NPCs Using NPC-Derived Organoids

(A) Immunofluorescence staining and **(B)** Quantification of SOX1+ (magenta) cells in organoids at days 30 (d30) and 180 (d180). Data represents mean ± SD, n=5 organoids per condition. **(C)** Immunofluorescence staining and **(D)** Quantification of SOX9+ (green) cells in organoids at days 30 (d30) and 180 (d180). Data represents mean ± SD, n=5 organoids per condition. **(E)** Immunofluorescence staining and **(F)** Quantification of Tbr1+ (pink) cells in organoids at days 30 (d30). Data represents mean ± SD, n=5 organoids per condition. **(G)** Immunofluorescence staining and **(H)** Quantification of SATB2+ (magenta) cells in organoids at days 180 (d180). Data represents mean ± SD, n=5 organoids per condition. **(I)** Immunofluorescence staining and **(J)** Quantification of GFAP (green) in organoids at days 180 (d180). Data represents mean ± SD, n=5 organoids per condition.

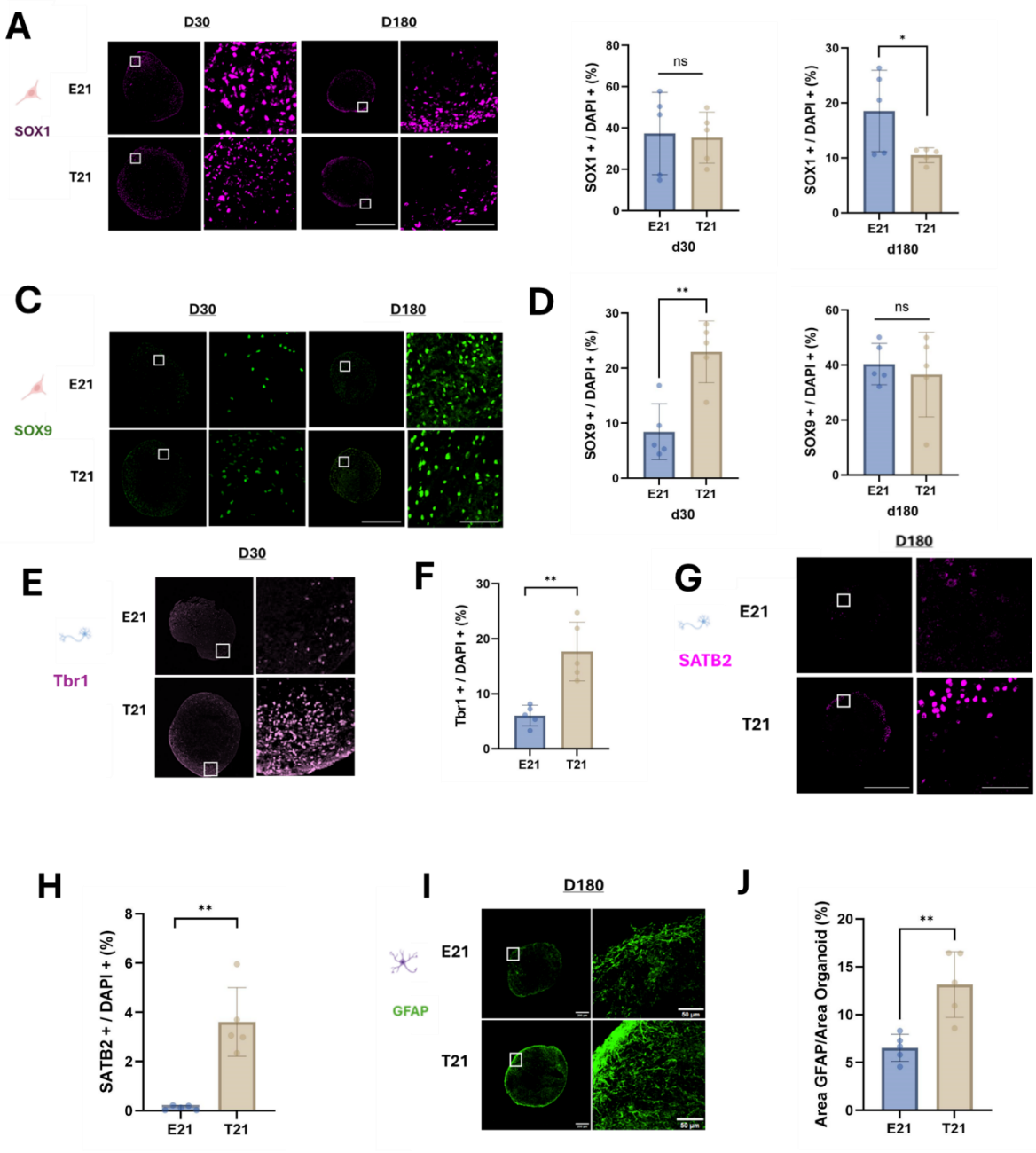
A
D30
D180
E21
SOX1
T21
SOX1 + / DAPI + (%)
ns
d30
*
d180
C
SOX9
D
**
SOX9 + / DAPI + (%)
E
Tbr1
F
Tbr1 + / DAPI + (%)
G
SATB2
H
SATB2 + / DAPI + (%)
I
GFAP
J
Area GFAP/Area Organoid (%)

REFERENCES

1. Oromendia, A. B. & Amon, A. Aneuploidy: implications for protein homeostasis and disease. *Disease Models & Mechanisms* **7,** 15–20 (2014).

2. Windsperger, K. & Hoehl, S. Development of Down Syndrome Research Over the Last Decades–What Healthcare and Education Professionals Need to Know. *Front. Psychiatry* **12,** 749046 (2021).

3. Kazemi, M., Salehi, M. & Kheirollahi, M. Down Syndrome: Current Status, Challenges and Future Perspectives. *Down Syndrome*

4. Alfonso, A. in *Conn's Translational Neuroscience* 545–552 (Elsevier, 2017). doi:10.1016/B978-0-12-802381-5.00039-7

5. UrbÃ¡n, N. & Guillemot, F. Neurogenesis in the embryonic and adult brain: same regulators, different roles. *Front. Cell. Neurosci.* **8,** (2014).

6. Ackerman, S. *Discovering the brain*. (National Academy Press, 1992).

7. Stiles, J. & Jernigan, T. L. The Basics of Brain Development. *Neuropsychol Rev* **20,** 327–348 (2010).

8. Homem, C. C. F., Repic, M. & Knoblich, J. A. Proliferation control in neural stem and progenitor cells. *Nat Rev Neurosci* **16,** 647–659 (2015).

9. Jiang, W., Chen, L. & Zheng, S. Global Reprogramming of Apoptosis-Related Genes during Brain Development. *Cells* **10,** 2901 (2021).

10. Tau, G. Z. & Peterson, B. S. Normal Development of Brain Circuits. *Neuropsychopharmacol* **35,** 147–168 (2010).

11. Kornack, D. R. & Rakic, P. Radial and horizontal deployment of clonally related cells in the primate neocortex: Relationship to distinct mitotic lineages. *Neuron* **15,** 311–321 (1995).

12. Lu, C., Garipler, G., Dai, C., Roush, T., Salome-Correa, J., Martin, A., Liscovitch-Brauer, N., Mazzoni, E. O. & Sanjana, N. E. Essential transcription factors for induced neuron differentiation. *Nat Commun* **14,** 8362 (2023).

13. Elkouris, M., Balaskas, N., Poulou, M., Politis, P. K., Panayiotou, E., Malas, S., Thomaidou, D. & Remboutsika, E. Sox1 Maintains the Undifferentiated State of Cortical Neural Progenitor Cells via the Suppression of Prox1-Mediated Cell Cycle Exit and Neurogenesis. *Stem Cells* **29,** 89–98 (2011).

14. Srinivasan, K., Leone, D. P., Bateson, R. K., Dobreva, G., Kohwi, Y., Kohwi-Shigematsu, T., Grosschedl, R. & McConnell, S. K. A network of genetic repression and derepression specifies projection fates in the developing neocortex. *Proc. Natl. Acad. Sci. U.S.A.* **109,** 19071–19078 (2012).

15. Sun, W., Cornwell, A., Li, J., Peng, S., Osorio, M. J., Aalling, N., Wang, S., Benraiss, A., Lou, N., Goldman, S. A. & Nedergaard, M. SOX9 Is an Astrocyte-Specific Nuclear Marker in the Adult Brain Outside the Neurogenic Regions. *J. Neurosci.* **37,** 4493–4507 (2017).

16. Bystron, I., Blakemore, C. & Rakic, P. Development of the human cerebral cortex: Boulder Committee revisited. *Nat Rev Neurosci* **9,** 110–122 (2008).

17. Liang, X. G., Hoang, K., Meyerink, B. L., Kc, P., Paraiso, K., Wang, L., Jones, I. R., Zhang, Y., Katzman, S., Finn, T. S., Tsyporin, J., Qu, F., Chen, Z., Visel, A., Kriegstein, A., Shen, Y., Pilaz, L.-J. & Chen, B. A conserved molecular logic for neurogenesis to gliogenesis switch in the cerebral cortex. *Proc. Natl. Acad. Sci. U.S.A.* **121,** e2321711121 (2024).

18. Antonarakis, S. E., Skotko, B. G., Rafii, M. S., Strydom, A., Pape, S. E., Bianchi, D. W., Sherman, S. L. & Reeves, R. H. Down syndrome. *Nat Rev Dis Primers* **6,** 9 (2020).

19. *Genomics, Proteomics, and the Nervous System*. **2,** (Springer New York, 2011).

20. Guidi, S., Bonasoni, P., Ceccarelli, C., Santini, D., Gualtieri, F., Ciani, E. & Bartesaghi, R. RESEARCH ARTICLE: Neurogenesis Impairment and Increased Cell Death Reduce Total Neuron Number in the Hippocampal Region of Fetuses with Down Syndrome: Hippocampal Hypocellularity in Down Fetuses. *Brain Pathology* **18,** 180–197 (2007).

21. Stagni, F., Giacomini, A., Emili, M., Guidi, S. & Bartesaghi, R. Neurogenesis impairment: An early developmental defect in Down syndrome. *Free Radical Biology and Medicine* **114,** 15–32 (2018).

22. Patkee, P. A., Baburamani, A. A., Kyriakopoulou, V., Davidson, A., Avini, E., Dimitrova, R., Allsop, J., Hughes, E., Kangas, J., McAlonan, G. & Rutherford, M. A. Early alterations in cortical and cerebellar regional brain growth in Down Syndrome: An in vivo fetal and neonatal MRI assessment. *NeuroImage: Clinical* **25,** 102139 (2020).

23. Jiwaji, Z. & Hardingham, G. E. Good, bad, and neglectful: Astrocyte changes in neurodegenerative disease. *Free Radical Biology and Medicine* **182,** 93–99 (2022).

24. Vacca, R. A., Bawari, S., Valenti, D., Tewari, D., Nabavi, S. F., Shirooie, S., Sah, A. N., Volpicella, M., Braidy, N. & Nabavi, S. M. Down syndrome: Neurobiological alterations and therapeutic targets. *Neuroscience & Biobehavioral Reviews* **98,** 234–255 (2019).

25. Hibaoui, Y., Grad, I., Letourneau, A., Sailani, M. R., Dahoun, S., Santoni, F. A., Gimelli, S., Guipponi, M., Pelte, M. F., Béna, F., Antonarakis, S. E. & Feki, A. Modelling and rescuing neurodevelopmental defect of D own syndrome using induced pluripotent stem cells from monozygotic twins discordant for trisomy 21. *EMBO Mol Med* **6,** 259–277 (2014).

26. Hill, E., Nagel, D., Parri, R. & Coleman, M. Stem cell-derived astrocytes: are they physiologically credible? *The Journal of Physiology* **594,** 6595–6606 (2016).

27. Kang, S., Chen, X., Gong, S., Yu, P., Yau, S., Su, Z., Zhou, L., Yu, J., Pan, G. & Shi, L. Characteristic analyses of a neural differentiation model from iPSC-derived neuron

according to morphology, physiology, and global gene expression pattern. *Sci Rep* **7,** 12233 (2017).

28. Meharena, H. S., Marco, A., Dileep, V., Lockshin, E. R., Akatsu, G. Y., Mullahoo, J., Watson, L. A., Ko, T., Guerin, L. N., Abdurrob, F., Rengarajan, S., Papanastasiou, M., Jaffe, J. D. & Tsai, L.-H. Down-syndrome-induced senescence disrupts the nuclear architecture of neural progenitors. *Cell Stem Cell* **29,** 116-130.e7 (2022).